International Journal of Remote Sensing
Vol. 33, No. 6, 20 March 2012, 1780–1798

Taylor & Francis
Taylor & Francis Group

Mapping alteration minerals at prospect, outcrop and drill core scales using imaging spectrometry

FRED A. KRUSE*†‡, RICHARD L. BEDELL‡§, JAMES V. TARANIK†‡, WILLIAM A. PEPPIN¶, OLIVER WEATHERBEE| and WENDY M. CALVIN†‡
†Department of Geological Sciences and Engineering, University of Nevada, Reno, NV 89557, USA
‡Arthur Brant Laboratory for Exploration Geophysics, University of Nevada, Reno, NV 89557, USA
§AuEx Ventures Inc., Reno, NV 89502, USA
¶SpecTIR, LLC, Reno, NV 89521, USA
|SpecTIR, LLC, Easton, MD 21601, USA

(*Received 22 December 2010; in final form 27 May 2011*)

Imaging spectrometer data (also known as 'hyperspectral imagery' or HSI) are well established for detailed mineral mapping from airborne and satellite systems. Overhead data, however, have substantial additional potential when used together with ground-based measurements. An imaging spectrometer system was used to acquire airborne measurements and to image in-place outcrops (mine walls) and boxed drill core and rock chips using modified sensor-mounting configurations. Data were acquired at 5 nm nominal spectral resolution in 360 channels from 0.4 to 2.45 μm. Analysis results using standardized hyperspectral methodologies demonstrate rapid extraction of representative mineral spectra and mapping of mineral distributions and abundances in map-plan, with core depth, and on the mine walls. The examples shown highlight the capabilities of these data for mineral mapping. Integration of these approaches promotes improved understanding of relations between geology, alteration and spectral signatures in three dimensions and should lead to improved efficiency of mine development, operations and ultimately effective mine closure.

1. Introduction

Imaging spectrometry, simultaneous measurement of continuous spectra and images in up to hundreds of spectral channels or bands, is a proven technology for identifying and mapping minerals based on their reflectance or emissivity signatures (Goetz *et al*. 1985). It has also become known as 'hyperspectral imagery' or 'HSI'. Imaging spectrometry's unique nature for remote mapping of surface materials relies on its capability to identify materials based on their electronic molecular spectral signatures in the visible and near-infrared (VNIR) and their vibrational molecular spectral signatures in the short-wave IR (SWIR) and long-wave IR (LWIR) spectral ranges (Clark *et al*. 1990, Hapke 1993) (figure 1). Mineral mapping using imaging spectrometer data is well established and routinely used for numerous geologic applications (Goetz

*Corresponding author. Email: fakruse@nps.edu. Now at: Naval Postgraduate School, Monterey, CA, USA.

International Journal of Remote Sensing
ISSN 0143-1161 print/ISSN 1366-5901 online
http://www.tandf.co.uk/journals
http://dx.doi.org/10.1080/01431161.2011.600350

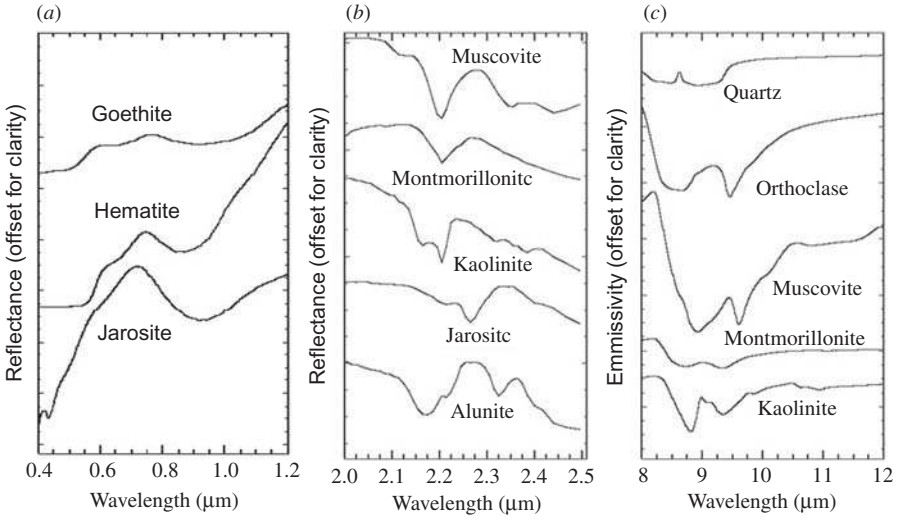

Figure 1. (*a*) Selected visible and near-infrared (VNIR) mineral signatures; (*b*) selected short-wave infrared (SWIR) mineral signatures; and (*c*) selected long-wave infrared (LWIR) mineral spectra. VNIR and SWIR spectra are from the USGS spectral library Splib06 (Clark *et al*. 2007). LWIR spectra are from the Johns Hopkins University spectral library (Salisbury *et al*. 1991). The USGS spectral library was used to make visual and numerical comparisons with airborne, rock outcrop and drill core hyperspectral data for mineral identification.

et al. 1985, Kruse 1988, Clark *et al*. 2003, Kruse and Perry 2009, Taranik and Aslett 2009). In addition to typical airborne and satellite hyperspectral data acquisitions, spectroscopy has also been used in a limited way for analysis of drill cores (Kowalik *et al*. 1991, Kruse 1996, Calvin *et al*. 2005) and for outcrop scanning (Kurz *et al*. 2008, 2009). More recently, concerted efforts have been directed at operational spectral logging of drill cores using automated methods (Mauger 2007, Huntington and Whitbourn 2010). Core imaging efforts are, however, still in the early stages of development (Kruse *et al*. 2010a,b). The research described here brings these airborne, core and outcrop imaging modalities together to demonstrate an integrated approach to mineral mapping for mine site exploration, evaluation and development.

1.1 *ProSpecTIR-VS scanner*

A wide variety of VNIR and SWIR airborne imaging spectrometers have been or are currently being flown (http://www.geo.unizh.ch/~schaep/research/apex/is_list.html). The ProSpecTIR-VS hyperspectral system operated by SpecTIR, LLC (www.spectir.com), is a custom-integrated system that incorporates Specim's (www.specim.fi) Airborne Imaging Spectrometer for Applications (AISA), Eagle (VNIR) and Hawk (SWIR) imaging spectrometers. The combination of these two high-performance sensors provides for the simultaneous acquisition of full hyperspectral data covering the 0.4–2.45 μm spectral range. The two imaging spectrometers are co-aligned and generate a single, full-spectrum data cube covering 320 pixels cross-track. In airborne operation, as a pushbroom instrument and utilizing a 24° scan and 0.075° (approximately 1.3 mrad) instantaneous field of view (IFOV), the system achieves spatial resolutions varying from 0.5 to 5 m depending upon altitude and platform speed. The

data collected for this experiment constitute spectral measurements in 360 spectral bands in total, covering the 0.4–2.45 μm spectral range at approximately 5 nm spectral resolution. The ProSpecTIR-VS sensor was operated in three different modes for the purposes of this research: (1) airborne overflight data at approximately 1 m spatial resolution, (2) core and rock-chip scans using a custom scanning bed and artificial (halogen) illumination at approximately 2 mm spatial resolution and (3) mine-wall scans using a truck-mounted scanning configuration and solar illumination at approximately 4 cm spatial resolution. ProSpecTIR data from all sources were calibrated by SpecTIR LLC to radiance using dark current correction, array normalization (flat fielding) and radiometric calibration using a Labsphere USS-2000-V uniform source (National Institute of Standards (NIST) – traceable integrating sphere) (personal communication, SpecTIR LLC, 2009). The resultant calibration produced VNIR/SWIR radiance data within ±5% of absolute radiance. Wavelength calibration was performed using an Oriel Cornerstone 130 1/8 m monochromator (Newport Corporation, Irvine, CA, USA). The central wavelength locations are known and certified within 0.5 nm accuracy.

1.2 *Trinity Mine site*

The area selected for study was the now inactive Trinity silver mine located approximately 150 km NE of Reno, NV, USA (40° 23′ 45″ N, 118° 36′ 40″ W) (figure 2). Access to the mine, cores/rock chips, core logs and elemental analysis for selected samples was provided by AuEx Ventures, Inc., Reno, NV, USA. The Trinity Silver Deposit was mined in the late 1980s by US Borax and actively mined for only 18 months. For one calendar year, it was the biggest silver producer in the USA (Hudson 2006).

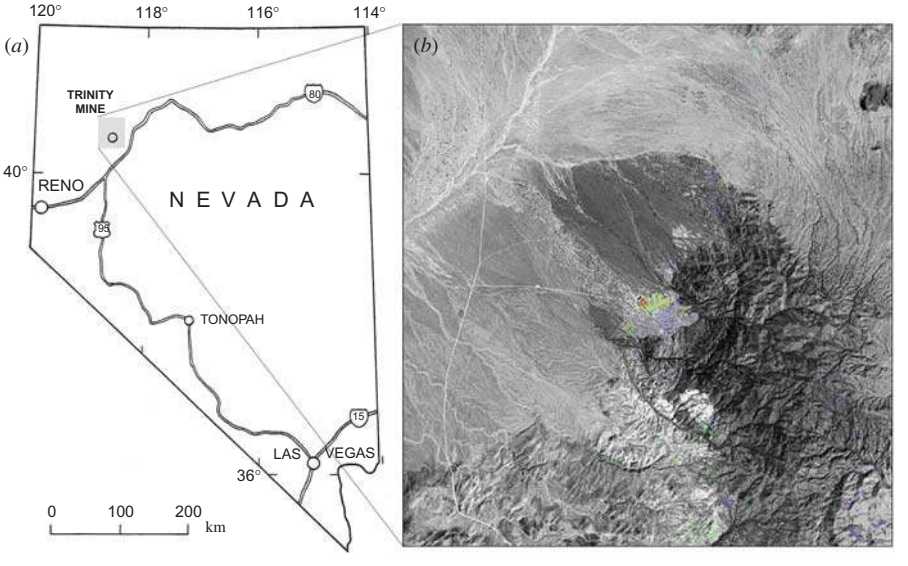

Figure 2. Trinity Mine location (*a*) and Landsat Thematic Mapper (TM) overview image (*b*). Grey-scale image is Landsat TM band 3 (0.66 μm). The Trinity Mine area is colour coded according to Landsat-mapped mineralogy: blue, clay; green, iron oxides; yellow to red, mixture of clay and iron oxides.
Note: Arcuate features to the east of the mine are suggestive of a possible intrusive complex.

Geologically, the deposit is hosted in a high tin rhyolite with silver selenides in breccias. This is very similar in occurrence to silver deposits in the Bolivian tin belt that includes some of the largest silver deposits in the world (Bedell, written communication, 2009). The age of mineralization was dated to be Oligocene (Argon-40/Argon-39 age of 25.111 ± 0.064 Ma) which is the same age as the Majuba Hill porphyry deposit to the north (Hudson *et al*. 2006, John and Muntean 2006). Structure in the pit is complex and not all relationships are understood; however, there are several N- and NE-trending gouge zones (Hudson 2006). Radial features visible on Landsat Thematic Mapper (TM) data suggest a larger intrusive complex at depth and ultimately this mineralization may be related to another porphyry system (Bedell, written communication, 2009) (figure 2). Clay alteration (probably illite, illite/smectite or muscovite based on field investigations) is generally associated with the NE- and N-trending gouge zones along faults, with rare silicification. Outside the gouge zones, alteration is generally weak (Hudson 2006). Sulphides are mainly in unoxidized gouge matrix and iron-oxide stained areas and correspond with higher oxide silver values, based on blast hole maps, atomic absorption (AA) elemental analysis, along with fire assay with a gravimetric finish of samples that exceeded 100 PPM silver as determined by US Borax (Hudson 2006). Association of oxide silver with iron oxides suggests transport of metals laterally from the gouge zones during supergene oxidation and deposition in the hanging wall.

2. Methods and data processing

2.1 *ProSpecTIR-VS airborne data acquisition*

Several flightlines of combined VNIR/SWIR ProSpecTIR-VS data were collected on 2 September 2009 at an approximate altitude above terrain of 750 m, achieving approximately 1 m spatial resolution. The ProSpecTIR-VS scanner as utilized for this acquisition was flown in a Cessna 206 aircraft without instrument stabilization (figure 3). Global Positioning System (GPS) coordinates, an onboard inertial navigation system (INS) and a 10 m National Elevation Dataset (NED) provide precision positioning information allowing geocorrection and geocoding to a typical geographic accuracy of

Figure 3. ProSpecTIR-VS hyperspectral scanner mounted in Cessna 206 aircraft.

less than two spatial pixels on the ground. The NED used here, however, is inadequate for such accuracy within the mine pit, because it was created before the pit existed. The imaging spectrometer data were calibrated to radiance using standard SpecTIR procedures traceable back to NIST standards and delivered as scaled radiance, using a gain to convert to integer format for storage purposes. On receipt, the scaling gain was inversely applied to convert to the original radiance values and the data were then corrected to reflectance using the Atmospheric CORrection Now (ACORN) atmospheric model (Kruse 2004) (see §2.4). The VNIR/SWIR data were analysed separately using endmember extraction and mixture tuned matched filtering (MTMF) to produce mineral maps (see §2.4) (Boardman 1998, Kruse *et al*. 2000). Results were geocorrected using the geometric model determined from the GPS/INS and combined to form a georeferenced mosaic (Boardman 1999).

2.2 *ProSpecTIR-VS core and rock-chip imaging*

The same ProSpecTIR-VS system was installed in a custom laboratory configuration to allow scanning of rock cores and rock chips, heretofore referred to as 'core'. The setup consists of a sensor mount, scanning bed, artificial illumination and computer control module (figure 4). Twenty-three core boxes and seven rock-chip trays were run sequentially through the imaging spectrometer at a distance of about 1 m under artificial (halogen) illumination. The raw spectral data were converted to radiance using the same methods as for the airborne imagery described above, providing high signal-to-noise data across the entire spectral range of the imager. A large Spectralon reflectance reference panel was run periodically with the core to allow correction to reflectance using a flat-field approach (dividing each pixel spectrum by the average Spectralon spectrum). This correction to Spectralon reflectance was done column by column due to the variation in cross-track lighting provided by the prototype system shown in the figure. Combined VNIR/SWIR test scans (~360 bands 0.4–2.45 μm) and several SWIR-only (236 bands, 0.98–2.45 μm) scans were performed. Only the SWIR data are shown here. The individual core box scans were combined into one continuous core image with full spectral coverage and the standardized endmember extraction and MTMF mineral analysis and mapping methods described in §2.4 were applied to produce full core mineral map images.

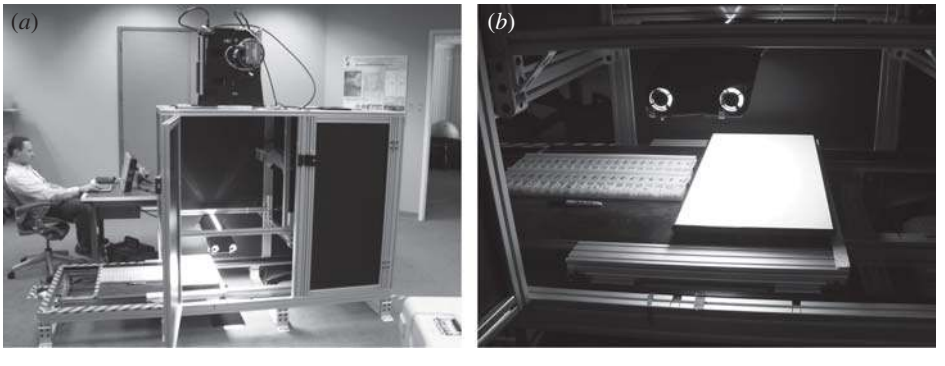

Figure 4. (*a*) ProSpecTIR-VS scanner in custom core scanning configuration; (*b*) scanning bed with rock chips and Spectralon panel.

2.3 *ProSpecTIR-VS mine-wall (outcrop) scans*

The same ProSpecTIR-VS scanner was vehicle mounted in a custom configuration on a rotating turntable, allowing side-to-side full-range spectral scanning at computer-controlled rates. The ~45° scan is indicated by the lines on the white base plate in figure 5. The 'along track' scan direction was determined by the moving stage, while the 'cross-track' dimension corresponds to the detector array swath. The GPS positions of the scanner and mine walls were noted and a laser rangefinder was used to determine the distance between the scanner and the outcrops. A 31 × 62 cm Spectralon reference panel was mounted on a tripod and placed within the scanned scene for the reflectance correction. Total setup and data acquisition was ~30 mins per site – a total of eight different scans were made, some were repeats of the same mine wall from different distances. The standardized, NIST-traceable SpecTIR procedures were followed for calibration of the raw ProSpecTIR data to radiance. The correction to reflectance was performed using the Spectralon Panel (see §2.4). The standardized endmember extraction and MTMF mineral analysis and mapping methods described in §§2.2 and 2.4 were applied to produce mine-wall mineral map images.

2.4 *Analysis methodology*

A standardized analysis approach was used for analysis of all of the ProSpecTIR imaging spectrometer data regardless of whether they were acquired using the airborne platform or from one of the two ground-based configurations. The basic concept

Figure 5. ProSpecTIR-VS scanner in custom configuration on rotating turntable in the vehicle for mine-wall (outcrop) scanning. The short-wave infrared (SWIR) instrument is on the left side of the box (round lens). The visible and near-infrared (VNIR) instrument is behind the rectangular port on the right.

was to extract characteristic spectra from the data themselves using convex geometry approaches (Boardman 1995, 1998) and then to map the distribution of these across the entire dataset to produce mineral maps of the spectrally predominant material. Calibrated radiance data were delivered by SpecTIR LLC. These were further corrected for atmospheric effects utilizing either an atmospheric model (in the case of the airborne data) or an empirical method utilizing a spectrally flat calibration target (in the case of the ground-based measurements). The reflectance correction step is a requirement for remote spectral measurement and analysis. Imaging spectrometer data are routinely calibrated to radiance by data providers using laboratory measurements validated by in-flight (or on-site) calibration experiments (Green *et al*. 2003). SpecTIR LLC applied these standardized procedures to produce the radiance data for this study. Radiance data from airborne systems are then usually corrected to reflectance utilizing the measured spectral images and atmospheric models such as the Moderate-Resolution Atmospheric Radiance and Transmittance Model (MODTRAN) and related imaging-spectrometer-specific correction software (Gao *et al*. 1993, Richter and Schläpfer 2002, Matthew *et al*. 2003, Kruse 2004). This approach produces excellent surface reflectance data without requiring the use of ground spectral measurements (Kruse 2004). The ACORN atmospheric model (Kruse 2004) was used to correct the Trinity Mine ProSpecTIR airborne data to reflectance. Atmospheric water vapour features near 0.9 and 1.1 μm (which are fully resolved using imaging spectrometer data) were used to estimate atmospheric water vapour concentration on a pixel-by-pixel basis. These estimates were used along with data characteristics (band centres and full-width-half-maximum radiometric responses) and acquisition parameters (ground elevation, flight altitude, site latitude/longitude, date and time) with the atmospheric model to produce a per-pixel reflectance corrected dataset. In the case of the ground-based core and outcrop measurements, a calibration panel of Spectralon with known spectral reflectance traceable to a NIST standard was included in each scan. The radiance data were corrected to reflectance by dividing each pixel radiance measurement by the radiance measurement for the calibration panel.

Spectral signatures in the atmospherically corrected imaging spectrometer data were used to find what minerals occur at the surface and how they are spatially distributed. The approach used here involved reducing the data to just a few key spectra that explained all of the data spectral variability, thereby defined as 'endmembers'. Geologic materials (and vegetation) mix at the surface (as aerial mixtures) in such a way that the mixed spectra are linear combinations of the endmember spectra occurring in a specific pixel (Boardman 1993, Boardman *et al*. 1995). Once endmembers were determined, their location and abundances were estimated and mapped using several spectral matching approaches (Green *et al*. 1988, Kruse *et al*. 1993a). Operationally, the method used for all of the ProSpecTIR datasets consisted of applying the following steps to the imaging spectrometer data (summarized in Kruse *et al*. (2000), additional references below):

(1) Correction of airborne imaging spectrometer data for atmospheric effects using the ACORN-MODTRAN-based atmospheric model (Kruse 2004). Correction of ground-based spectral scans (core and outcrop) utilizing a 'flat-field' correction derived by measuring a Spectralon panel simultaneously with the mineral scan, then dividing each pixel spectrum by the Spectralon measurement.

(2) Spectral compression, noise suppression and dimensionality reduction using the minimum noise fraction (MNF) transformation (Green *et al*. 1988, Boardman 1993).
(3) Determination of endmember occurrences using convex geometric methods (pixel purity index – 'PPI') (Boardman 1995).
(4) Extraction of endmember spectra using *n*-dimensional (*n*-D) scatter plotting and visualization (Boardman and Kruse 1994).
(5) Identification of mineral endmember spectra using visual inspection, automated identification and spectral library comparisons (Kruse *et al*. 1993b, Kruse 2008).
(6) Production of mineral maps using MTMF, a partial linear spectral unmixing procedure that finds and maps specific minerals constrained by mixing with a composite (unknown) background (Boardman 1998).

The imaging spectrometer mineral mapping results are typically presented as multiple grey-scale abundance images (one per endmember) and/or combined as a single classified image utilizing a combination of the matched filter (MF) abundance image and a mixture feasibility image (infeasibility score) showing the spectrally predominant material (Boardman 1998, Kruse *et al*. 2000).

3. Results

The following descriptions and figures illustrate the application of the above analysis approaches to the various ProSpecTIR datasets. Only the SWIR data results are shown. While these methods do allow for mapping of multiple minerals (mineral assemblages), and of mineral abundances, only the spectrally predominant mineral for each pixel is shown for the purposes of this demonstration. In the referenced figures, map colours have been standardized so that all of the mineral maps can be cross-compared, regardless of the data source (airborne vs. core scans vs. mine-wall scans).

3.1 *ProSpecTIR-VS Trinity Mine overflight*

The overhead ProSpecTIR SWIR mineral map principally shows the spatial association of illite/muscovite with the mined open pit (figure 6, right). SWIR minerals mapped are mostly limited to the mined exposures on benches, but there are some possible extensions (of illite/muscovite 1 and particularly of jarosite) away from the mine. The primary distribution (green in figure 6) corresponds to the signature for 'illite/muscovite 1', having a main absorption feature position near 2.196 μm. Shift of this absorption feature to wavelengths short of 2.2 μm has been shown to be correlated with increased Al content in muscovite, usually related to high-temperature hydrothermal alteration (Duke 1994, Martinez-Alonso *et al*. 2002). There is also a second presumably lower temperature illite/muscovite occurrence (illite/muscovite 2) with the main feature near 2.203 μm (dark green in figure 6). Also note the partial association of jarosite principally with the lowest central floor of the open pit ('A' on figure 7). This is interpreted to correspond with the exposure of oxidized pyrite at the mined surface interface and may be indicative of proximity to un-mined 'reduced silver ore' containing pyrite and other sulphides (Bedell, personal communication, 2009) (figure 7).

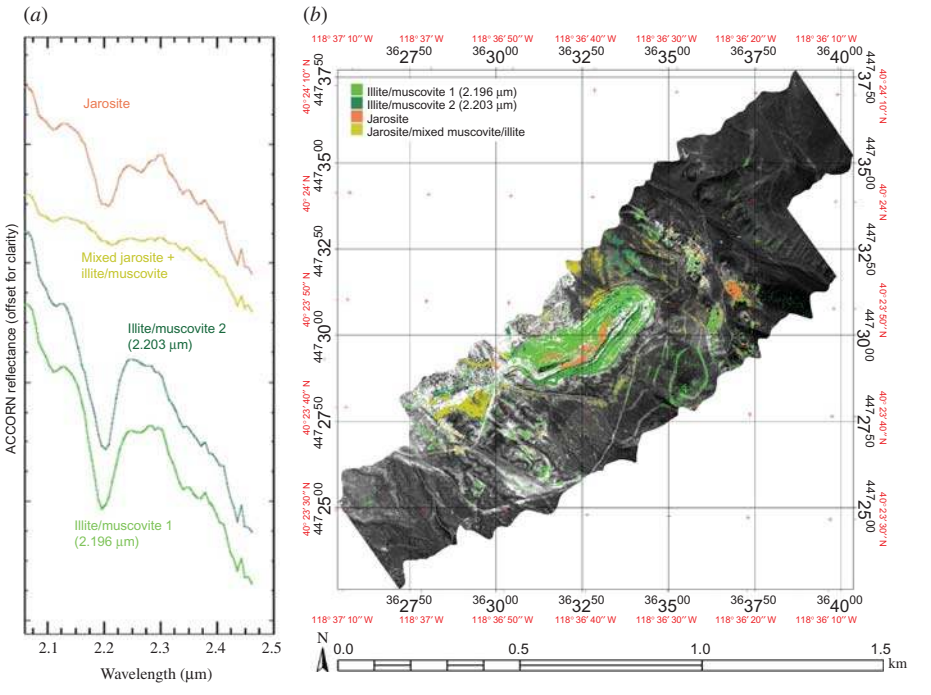

Figure 6. Trinity Mine overhead ProSpecTIR imaging spectrometer results. (*a*) Spectral end-members extracted from the data, (*b*) mixture tuned matched filtering (MTMF) mineral map showing spectrally predominant mineral at each pixel.

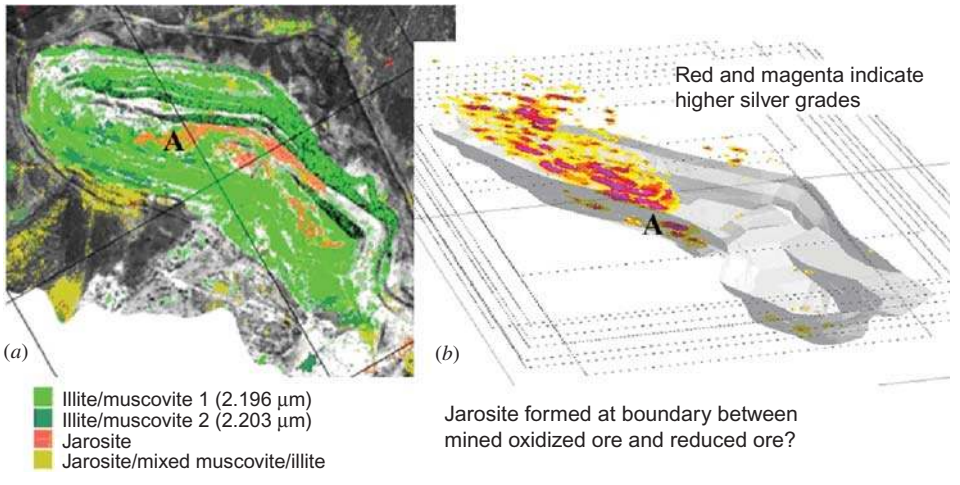

Figure 7. Comparison of the ProSpecTIR short-wave infrared (SWIR) mineral map for the bottom of the Trinity Mine pit (extracted from figure 6) to 3D plot of mined silver ore grade. Colours on mineral map (*a*) match figure 6. Red and magenta colours on ore grade plot (*b*) indicate higher silver grades. Note apparent partial correspondence at approximate location 'A' between bottom of mined high-grade ore in (*b*) and the centre part of the jarosite zone shown in (*a*). North–south index lines on (*a*) run from upper right to lower left and (*b*) shown in approximately the same orientation.

3.2 *ProSpecTIR-VS rock chip scans*

Two separate types of 'core' were analysed: (1) reverse-circulation rock chips in plastic trays and (2) split core in cardboard boxes. Figure 8 shows the physical layout for the boxed rock chips and seven separate boxes scanned, two at a time. The core images were manually extracted from the lid images using interactive spatial subsetting (an automated procedure could have been designed, but was not attempted for this demonstration). The core images were then stacked by depth into one spectral image cube (figure 9) and analysed using the approaches described previously. The spectral endmembers extracted using the MNF, PPI, *n*-D visualization procedures are similar to those extracted for the overhead imaging spectrometer data, with the addition of kaolinite (not seen in the overhead data) (figure 9). Mineral distribution in the core was mapped using MTMF. Again, the principal mineralogy is the short-wavelength (2.196 μm) illite/muscovite. Some jarosite mixed with illite/muscovite was observed in the core image, but no substantial occurrences of jarosite by itself. Comparison of the mapped mineralogy with core logs provided by AuEx showed general correspondence between scan-identified clay and logged clay; however, the scan mineralogy is much more detailed than that described in the manual logs. There is also some correlation with elemental analysis, particularly the association of illite/muscovite bordered by kaolinite with transition from low- to high-silver (Ag) values (for some but not all occurrences) (figure 9). It is suggested that the kaolinite results from acid-sulphate (supergene) alteration at the boundaries between sulphides and oxidized materials.

3.3 *ProSpecTIR-VS boxed core scans*

The second type of core analysed was split core in cardboard boxes. Figure 10 shows the extracted mineral endmembers from all of the boxed core and the MTMF mineral maps for the individual core boxes (though they were all analysed simultaneously as one imaging spectrometer cube). Twenty-three separate boxes were scanned and

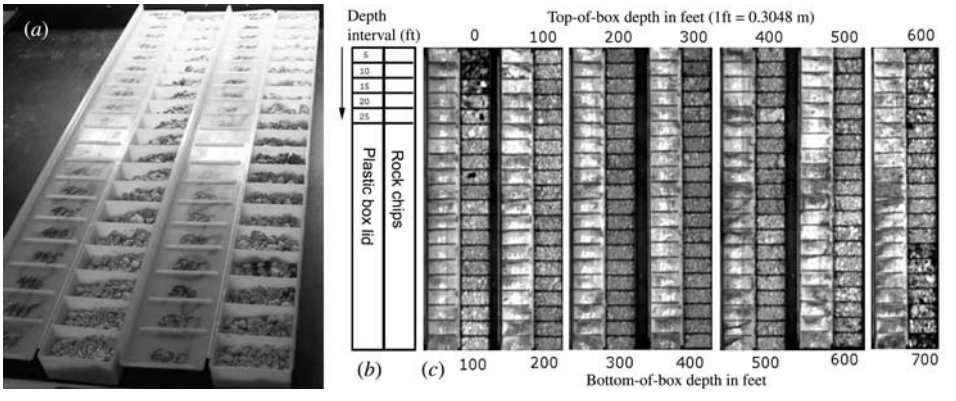

Figure 8. (*a*) Photograph of two rock-chip boxes side by side. (*b*) Diagram shows box layout for reverse-circulating rock chips. The chips are in white plastic boxes and the snap lids are open to the left. The second column contains the actual rock chips at approximately 1.5 m (5 ft) spacing. (*c*) Seven boxes of rock chips were scanned for drill hole 'TD006', two per scan, corresponding to a total depth of approximately 215 m (700 ft). Chips were acquired and depths originally measured in feet and this is how they are marked in the boxes and on the right-hand figure. One foot equals approximately 0.3048 m. Band 195 at 2.196 μm shown.

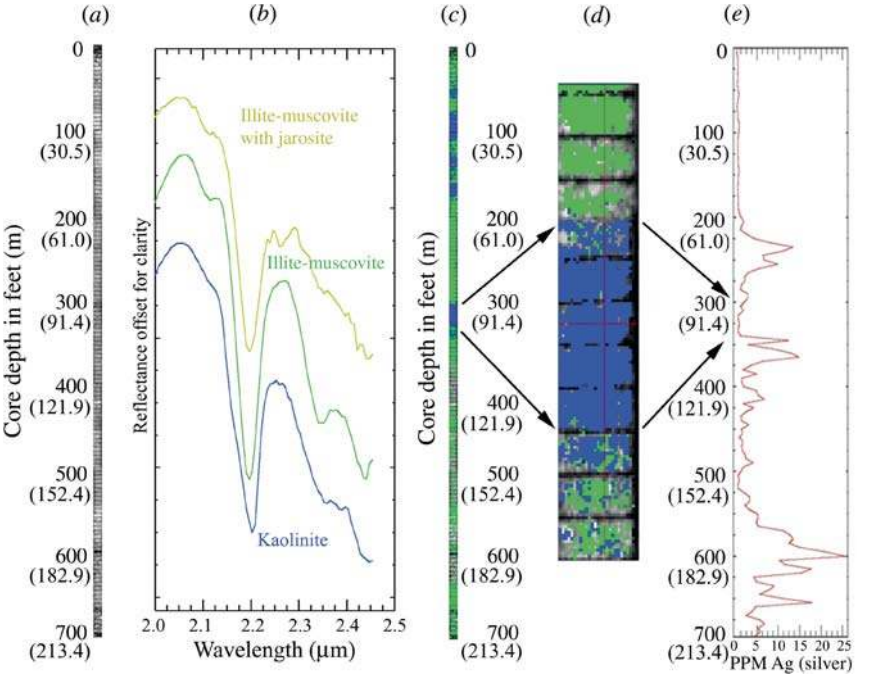

Figure 9. Scanned core TD006 image, spectral mineralogy and associated silver analysis are shown. The left grey-scale image (*a*) is the full 700 ft (213.4 m) of core stacked by depth (band 195 at 2.196 μm is shown). (*b*) Endmember spectra extracted from the core data using the methods in the text. (*c*) Mixture tuned matched filtering (MTMF) mineral map of the entire 700 ft (213.4 m) of core. Colours correspond to the endmember colours shown in (*b*). (*d*) Zoomed portion of the mineral map around one of the kaolinite occurrences. Arrows from (*c*) to (*d*) show approximate depth relationship of the subset image to the full core. (*e*) Silver (Ag) concentration in PPM down the core as determined using atomic absorption (AA) elemental analysis. Arrows from (*d*) to (*e*) indicate approximate depth correlations between the mineral map subset and the elemental analysis. Chips were acquired and depths originally measured in feet and this is how they are marked in the core boxes and in the figure. Approximate equivalent depths in metres are shown in parentheses.

analysed. Cross-comparison of the mapped mineralogy with core logs provided by AuEx again shows general correspondence (e.g. scan clay and scan jarosite correlated with log clay and log sulphides, respectively); however, the core scan mineralogy is again much more detailed than that described in the manual logs. In addition, as the data analysis methods are totally objective (and potentially quantitative), they have substantive advantages over manual core logging.

Figure 11 shows the layout for the imaging spectrometer cube of stacked boxes along with a zoomed portion of several individual core boxes. All of the individual scans were combined into one data cube and spectral endmembers were extracted using the MNF, PPI, *n*-D visualizer approach previously described. The same mineralogy was detected and identified as for the reverse-circulating rock chips and for the overhead imagery (with the addition of kaolinite). Again, there appears at least a partial association between specific mineralogy (kaolinite and jarosite) with elevated silver values. The cores between approximately 180 and 190 ft (55–58 m) depth illustrate a well-developed kaolinite and jarosite zonation, bounded on either side by illite/muscovite

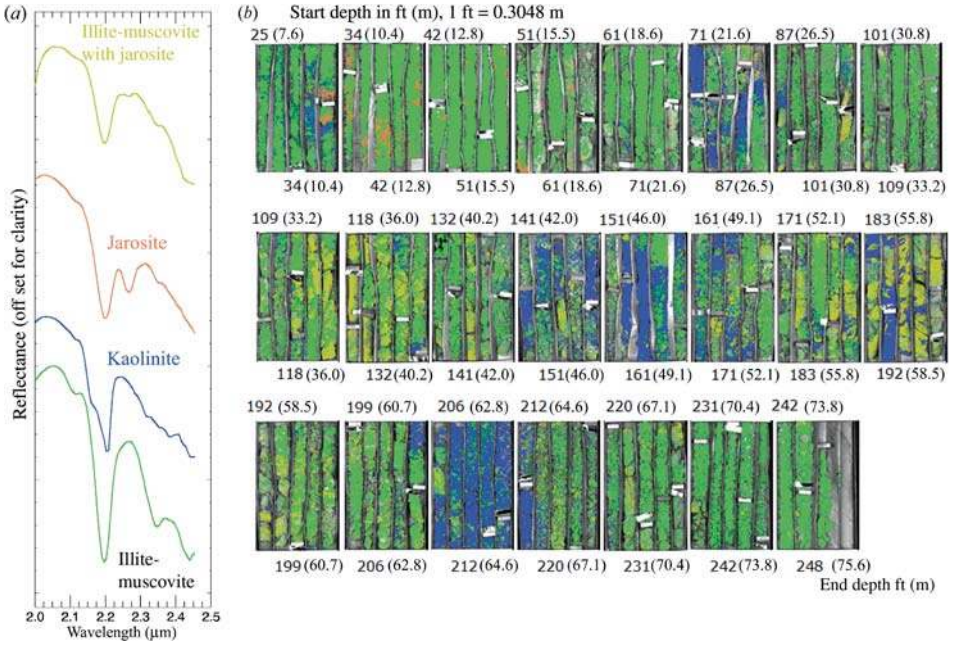

Figure 10. (*a*) Spectral endmembers extracted from the total boxed core dataset for drill hole TS07-25. (*b*) Colour-coded images for 23 separate boxes of core analysed using the mixture tuned matched filtering (MTMF) approach. Core depth increases from the upper left to the lower right of each box – approximately 248 ft (76 m) total shown. The depth for the top of each box is marked adjacent to the upper left corner of the box. The depth for the bottom of each box is marked adjacent to the lower right corner of the box. The colours for the analysed core correspond to those shown for the mineral endmembers. Note the associations of kaolinite and jarosite (or mixed jarosite/illite-muscovite) in some of the cores. Cores were acquired and depths originally measured in feet and this is how they are marked in the core boxes and in the figure. Approximate equivalent metre depths are shown in parentheses. One foot equals 0.3048 m.

and this association is correlated with high known silver values in the cores in this depth range. The presence of these two minerals indicates acidic conditions in the hydrothermal fluids and points to probable association of pyritic (sulphide) materials and specific mineralogy. It leads to the conclusion that the imaging spectrometer data can be used to map out probable contacts between reduced sulphides and oxidized materials.

3.4 *ProSpecTIR-VS mine-wall scans*

The ProSpecTIR mine-wall scans were analysed using the same approach as for the overhead flight data and the core scans. A total of eight different scans were acquired for a variety of mine-wall locations, with some repeats at varying distances from the wall. Figure 12 shows a scan acquired from approximately 38 m (approximately 4 cm spatial resolution). Correction to reflectance was accomplished using the in-scene Spectralon panel, and the previously described MNF, PPI, *n*-D visualizer data analysis sequence was used to extract endmembers. Note that it is important when designing a plan for surveying the entire site (or specific wall orientations) to align solar

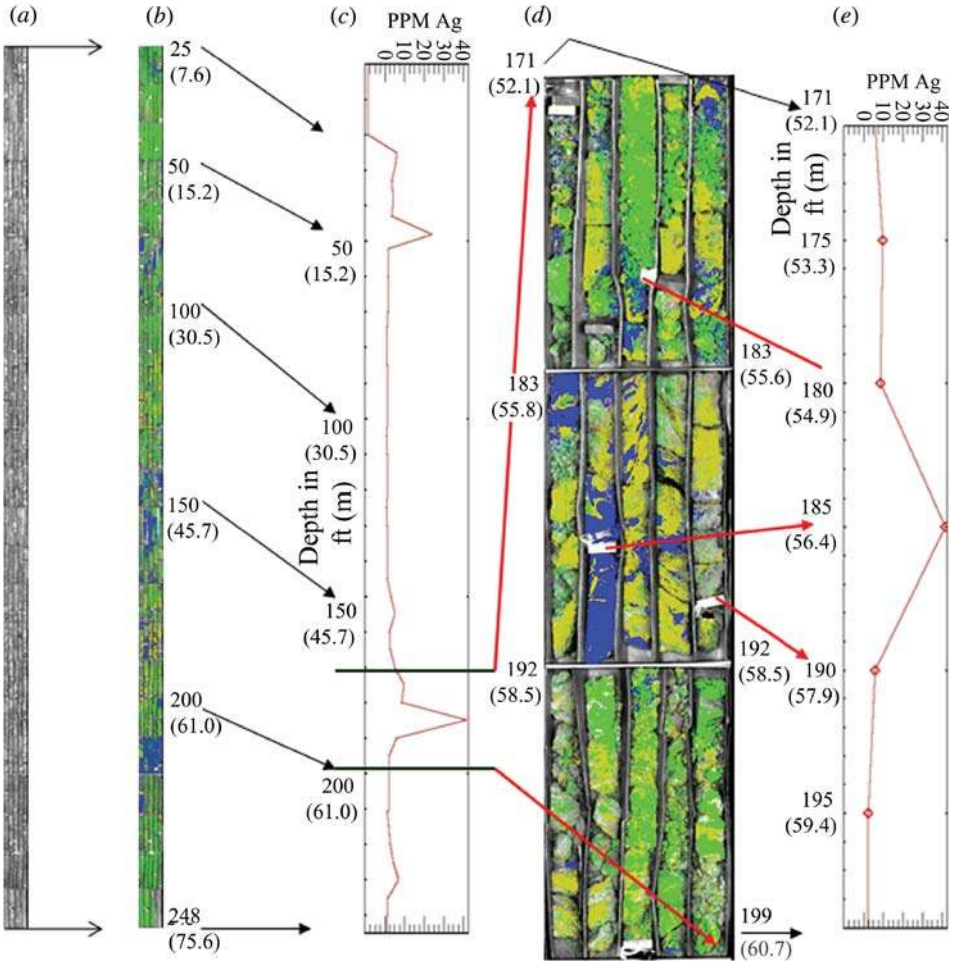

Figure 11. A variety of different representations of the scanned boxed core and mineralogy are shown. The left image (*a*) is the full 248 ft (76 m) of core stacked by box (band 195 at 2.196 μm image shown). (*b*) Full core mixture tuned matched filtering (MTMF) mineral map in box-stacked format. (*c*) Full core silver (Ag) analysis in PPM as determined using atomic absorption (AA) elemental analysis. (*d*) Zoomed portion of the core associated with elevated silver values. Core depth increases from the upper left to the lower right of each box. The corresponding zoomed silver analysis is shown in (*e*). Arrows trace approximate depth relationships. Each box contains a range of depths, so it is not a straight depth-to-image *Y*-position relationship. Following the arrows, note the association of kaolinite and mixed jarosite/illite-muscovite with the higher silver values. This again suggests to us an association of more acidic conditions with the boundaries between areas containing sulphides and more oxidized materials. Cores were acquired and depths originally measured in feet and this is how they are marked in the core boxes and in the figure. Approximate corresponding depths in metres are shown in parenthesis. One foot equals approximately 0.3084 m.

illumination and data collection times. For example, scan the west wall in the morning (east illumination) and the east wall in the afternoon (west illumination). It can be seen from figure 12 (left) that basically the same endmembers were detected as for the over-flights and cores; however, in this case, a reduced sulphide occurrence was scanned

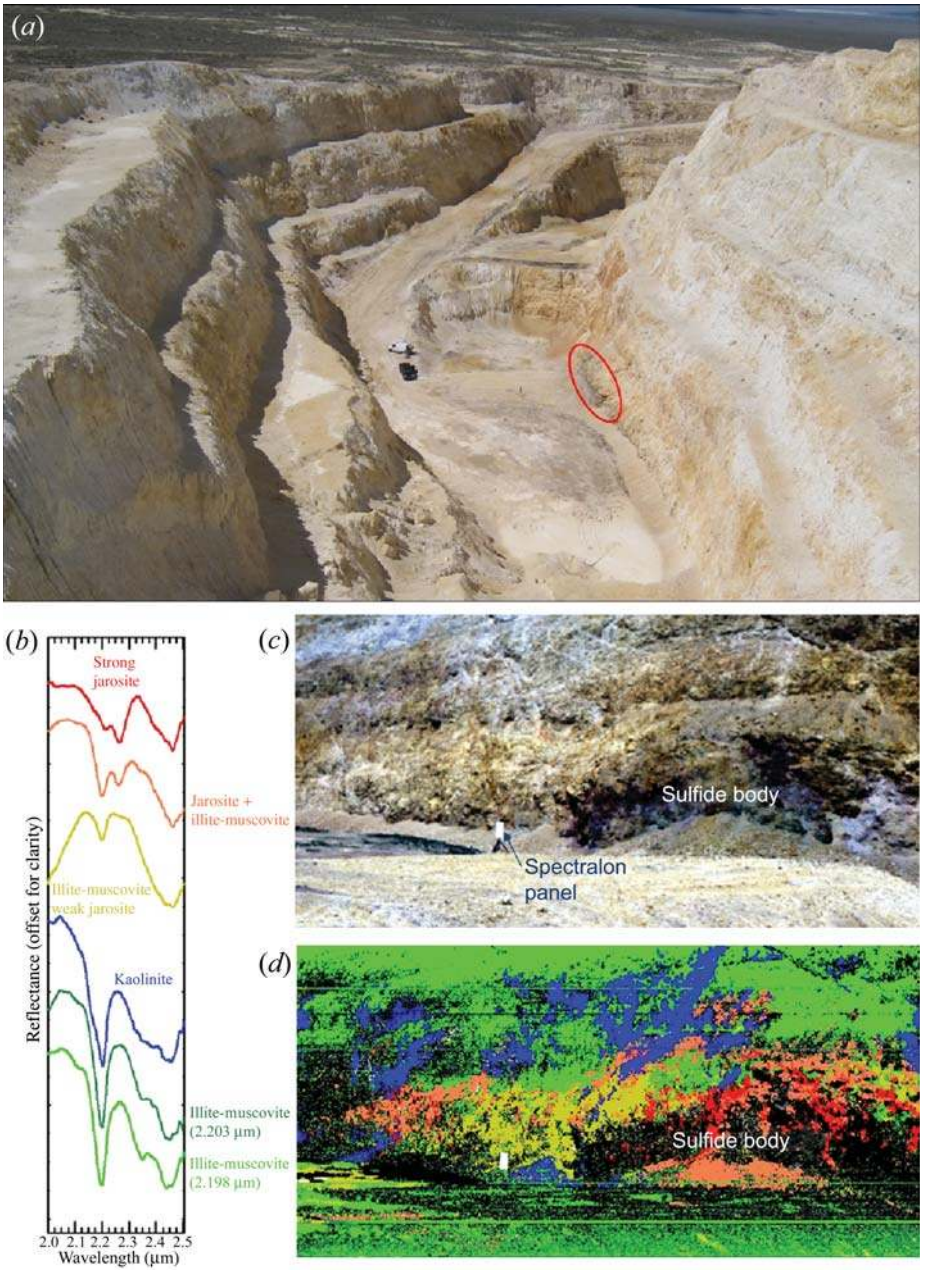

Figure 12. Mine-wall scan number 1145 for scan site 1 at the Trinity Silver Mine, Pershing County, NV, USA. Data were acquired on 7 May 2009 at 11:45 am local time using solar illumination. (*a*) Oblique photograph showing location of scan vehicle (white truck) and scanned area (circled in red). View from scanner to mine wall is from SE to NW. (*b*) Mineral endmember spectra extracted from the imaging spectrometer data cube utilizing the standardized approach. (*c*) True colour scanned mine-wall image (0.65, 0.55, 0.45 μm) (RGB). (*d*) MTMF SWIR mineral map produced from the mine-wall scan using the endmember spectra in (*b*). Image colours match the endmember spectra colours. Note zoned mineralogy around the dark, labelled sulphide occurrence and the linear nature of some of the kaolinite occurrences indicating probable association with structures (faults or fractures).

from only a few metres away and with approximately 4 cm spatial resolution. The wall scans produced detailed mineral mapping results and a view of the mineralogy (associated with sulphides) not available from any other source. The mine-wall mineral map shows the distribution of illite-muscovite, jarosite and kaolinite with respect to the sulphide area (dark unmapped areas labelled on figure 12). There is a clear relationship between the best jarosite signatures and the central part of the sulphide outcrop. Jarosite occurs roughly in zones of decreasing alteration away from centre of the exposed sulphides. This result confirms extensive documentation of similar relations by Swayze *et al*. (1996) and Coulter (2006) for sulphide deposits both naturally occurring and associated with mining activities. It should also be noted that kaolinite is associated with the periphery of the sulphide exposure and appears to extend along fractures away from the central, unaltered area, indicating lateral movement of acidic fluids.

4. Discussion and conclusions

This research provides a technology demonstration of imaging spectrometer data applied to several levels of mineral mapping for geological characterization. A ProSpecTIR-VS hyperspectral scanner was used to acquire 360-band airborne imaging spectrometer data at nominal 5 nm spectral resolution and 1 m spatial resolution in the 0.4–2.45 μm range. The same sensor, configured in a laboratory setting using artificial (halogen) illumination was used to measure rock-chip trays and boxed core with approximately 2 mm spatial resolution and the same spectral resolution from a distance of 1 m. Finally, the ProSpecTIR-VS sensor was vehicle mounted on a rotating turntable to scan approximately 45° horizontally to measure mine walls (outcrop) from 15 to 250 m distance. The mine-wall example shows approximately 4 cm spatial resolution.

Standardized analysis approaches typically used for analysis of airborne hyperspectral datasets were applied without modification to the overflight data, core scans and mine-wall scans. Representative spectral endmembers were extracted from the HSI data and used to map the spatial distribution of specific minerals in the airborne data, with depth in the rock chip and core data, and vertically and horizontally in the mine-wall scans. MTMF was used to locate specific minerals, determine their relative abundances and map their spatial distributions.

The airborne mineral mapping results show the distribution of surface mineralogy, highlighting the association of most alteration with the Trinity Mine open pit exposures. The mineralogy mapped consisted of two varieties of illite-muscovite, one a probable high-temperature aluminium hydroxide (AlOH) substituted alteration mineral. The presence and distribution of jarosite on the benches and bottom of the open pit was also mapped and appears to correlate with mined areas of high-grade silver ore. This conforms with communications by the mine owner (AuEx) that mining was stopped at the oxidized versus reduced ore interface (Bedell, personal communication, 2009). The presence of jarosite in the mine pit indicates the probable presence of near-surface sulphides (likely pyrite). Some additional new areas of interest due to jarosite were also identified outside the pit.

Core and rock-chip mapping allows detailed mineral characterization with depth for specific locations. The MTMF mineral mapping, combined with interactive analysis of the mineralogy using linked spatial-spectral browsing confirms similar mineralogy to that exposed at the surface. Areas of kaolinite and jarosite in the cores appear

to indicate boundaries between reduced versus oxidized materials and correspond to elevated silver values.

Mineral maps produced for mine-wall scans show similar mineralogy and relationships to those observed for the airborne and core HSI data. One scan of a known sulphide occurrence shows clearly zoned jarosite alteration decreasing in intensity away from the centre of the exposed sulphides. There is also a strong relationship between structure and mineralogy in the form of linear alignments of kaolinite radiating from the reduced area. The presence of this mineral assemblage indicates acid-sulphate conditions surrounding the sulphides.

Synthesis of all of the imaging spectrometer dataset results for the Trinity Mine site provides more detailed alteration mapping than was previously available. The results provide new insight to relations between alteration, structure and ore in three dimensions. This effort demonstrates the feasibility of using imaging spectrometers in a variety of mapping modes for improved mineral mapping. Results suggest that these approaches can be an effective operational tool for exploration and determination of mine geology and alteration. It is expected that the new information provided will lead to improved efficiency of mine development, operations and ultimately effective mine closure.

Acknowledgements

The ProSpecTIR data were collected by SpecTIR, LLC, Reno, NV, USA. Additional information is available at http://www.spectir.com. Trinity Mine access, core and logs and supporting data were provided by AuEx Ventures, Reno, NV, USA. Additional information is available at http://www.auexventures.com. The ACORN software was provided by Imspec, LLC (www.imspec.com). This research was sponsored by the Arthur Brant Endowment for Exploration Geophysics, which supports the UNR Arthur Brant Laboratory for Exploration Geophysics (ABLE), see http://www.mines.unr.edu/able/.

References

Boardman, J.W., 1993, Automated spectral unmixing of AVIRIS data using convex geometry concepts. In *Summaries of the 4th JPL Airborne Geoscience Workshop*, 25–29 October 1993, Washington, DC (Pasadena, CA: Jet Propulsion Laboratory), Vol. 1, 93-26, pp. 11–14.

Boardman, J.W., 1995, Analysis, understanding and visualization of hyperspectral data last convex sets in n-space. In *Proceedings of the SPIE Defense and Security*, Orlando, FL (Bellingham, WA: The International Society for Optical Engineering), pp. 14–22.

Boardman, J.W., 1998, Leveraging the high dimensionality of AVIRIS data for improved sub-pixel target unmixing and rejection of false positives: mixture tuned matched filtering. In *Summaries of the 7th Annual JPL Airborne Geoscience Workshop*, 12–16 January 1998, Pasadena, CA (Pasadena: Jet Propulsion Laboratory), p. 55.

Boardman, J.W., 1999, Precision geocoding of low altitude AVIRIS data: lessons learned in 1998. In *Proceedings of the 8th Annual JPL Airborne Earth Science Workshop*, 8–11 February 1999, Pasadena, CA (Pasadena, CA: Jet Propulsion Laboratory), pp. 63–68.

Boardman, J.W. and Kruse, F.A., 1994, Automated spectral analysis: a geological example using AVIRIS data, northern Grapevine Mountains, Nevada. In *Proceedings of the Tenth Thematic Conference, Geologic Remote Sensing*, 9–12 May 1994, San Antonio, TX (Ann Arbor, MI: Environmental Research Institute of Michigan), pp. I-407–I-418.

Boardman, J.W., Kruse, F.A. and Green, R.O., 1995, Mapping target signatures via partial unmixing of AVIRIS data. In *Summaries of the 5th Annual JPL Airborne Earth Science Workshop*, 23–26 January 1995, Pasadena, CA (Pasadena: Jet Propulsion Laboratory), pp. 23–26.

Calvin, W.M., Kratt, C. and Faulds, J.E., 2005, Infrared spectroscopy for drillhole lithology and mineralogy. In *Proceedings of the Thirtieth Workshop on Geothermal Reservoir Engineering Stanford University,* 31 January–2 February 2005, Stanford, CA (SGP-TR-176).

Clark, R.N., King, T.V.V., Klejwa, M., Swayze, G. and Vergo, N., 1990, High spectral resolution reflectance spectroscopy of minerals. *Journal of Geophysical Research*, **95**, pp. 12653–12680.

Clark, R.N., Swayze, G.A., Livo, K.E., Hoefen, T., Kokaly, R.F., Sutley, S.J., Dalton, J.B., Mcdougal, R.R. and Gent, C.A., 2003, Imaging spectroscopy: earth and planetary remote sensing with the USGS Tetracorder and expert systems. *Journal of Geophysical Research*, **108**, pp. 5–1–5–44.

Clark, R.N., Swayze, G.A., Wise, R., Livo, E., Hoefen, T., Kokaly, R. and Sutley, S.J., 2007, USGS digital spectral library splib06a. US Geological Survey, Digital Data Series 231. Available online at: http://speclab.cr.usgs.gov/spectral.lib06

Coulter, D.W., 2006, Remote sensing analysis of alteration mineralogy associated with natural acid arainage in the Grizzly Peak Caldera, Sawatch Range, Colorado. Unpublished PhD dissertation, Colorado School of Mines, Golden, CO, USA, 146 p.

Duke, E.F., 1994, Near infrared spectra of muscovite, Tschermak substitution, and metamorphic reaction progress: implications for remote sensing. *Geology*, **22**, pp. 621–624.

Gao, B.C., Heidebrecht, K.B. and Geotz, A.F.H., 1993, Derivation of scaled surface reflectances from AVIRIS data. *Remote Sensing of Environment*, **44**, pp. 165–178.

Goetz, A.F.H., Vane, G., Solomon, J.E. and Rock, B.N., 1985, Imaging spectrometry for earth remote sensing. *Science*, **228**, pp. 1147–1153.

Green, A.A., Berman, M., Switzer, P. and Craig, M.D., 1988, A transformation for ordering multispectral data in terms of image quality with implications for noise removal. *IEEE Transactions on Geoscience and Remote Sensing*, **26**, pp. 65–74.

Green, R.O., Chrien, T.G. and Pavri, B., 2003, On-orbit determination of the radiometric and spectral calibration of Hyperion using ground, atmospheric and AVIRIS underflight measurements. *IEEE Transactions on Geoscience and Remote Sensing*, **41**, pp. 1194–1203.

Hapke, B., 1993, *Theory of Reflectance and Emittance Spectroscopy* (Cambridge: Cambridge University Press).

Hudson, D.M., 2006, *Geologic Observations of the Trinity Silver Open Pit Mine, Pershing County, Nevada*. AuEx Ventures internal report, 38 p. (prepared for Piedmont Mining Company, Inc.).

Hudson, D.M., John, D.A. and Fleck, R.J., 2006, Geology, geochemistry, and geochronology of epithermal gold-silver deposits in the Seven Troughs district, Pershing County, Nevada. *Geological Society of Nevada Special Publication*, **42**, pp. 110–126.

Huntington, J. and Whitbourn, L.B., 2010, The AuScope national virtual core library – establishment and achievements. In *Program with Abstracts, 3D Mineral Spectroscopy of the Earth's Skin, The 1st National Virtual Core Library Symposium*, 8–9 July 2010, Canberra, ACT, Australia. Available online at: http://www.auscope.org.au/content.php/category/id/27

John, D.A. and Muntean, J., 2006, Summary of characteristics of tertiary metallic mineral deposits in the Lovelock area, northwestern Nevada. *Geological Society of Nevada Special Publication*, **42**, pp. 60–72.

Kowalik, W.S., Sabins, F.F., Corea, W.C. and Alameda, G.K., 1991, Multispectral scanning and digital processing of well cores. In *Proceedings of the Eighth Thematic Conference*

on Geologic Remote Sensing, Ann Arbor, MI (Ann Arbor: Environmental Research Institute of Michigan).

KRUSE, F.A., 1988, Use of airborne imaging spectrometer data to map minerals associated with hydrothermally altered rocks in the northern Grapevine Mountains, Nevada and California. *Remote Sensing of Environment*, **24**, pp. 31–51.

KRUSE, F.A., 1996, Identification and mapping of minerals in drill core using hyperspectral image analysis of infrared reflectance spectra. *International Journal of Remote Sensing*, **17**, pp. 1623–1632.

KRUSE, F.A., 2004, Comparison of ATREM, ACORN, and FLAASH atmospheric corrections using low-altitude AVIRIS data of Boulder, Colorado. In *Proceedings of the 13th Jet Propulsion Laboratory Airborne Geoscience Workshop,* 31 March–2 April 2004, Pasadena, CA (Pasadena: Jet Propulsion Laboratory).

KRUSE, F.A., 2008, Expert system analysis of hyperspectral data. In *Proceedings of the SPIE Defense and Security, Algorithms and Technologies for Multispectral, Hyperspectral, and Ultraspectral Imagery XIV*, 16–18 March 2008, Orlando, FL (Bellingham, WA: The International Society for Optical Engineering).

KRUSE, F.A., BOARDMAN, J.W. and LEFKOFF, A.B., 2000, Extraction of compositional information for trafficability mapping from hyperspectral data. In *Proceedings of the SPIE International Symposium on AeroSense*, 24–28 April 2000, Orlando, FL (Bellingham, WA: The International Society for Optical Engineering), Vol. 4049, pp. 262–273.

KRUSE, F.A., LEFKOFF, A.B., BOARDMAN, J.B., HEIDEBRECHT, K.B., SHAPIRO, A.T., BARLOON, P.J. and GOETZ, A.F.H., 1993a, The spectral image processing system (SIPS) – interactive visualization and analysis of imaging spectrometer data. *Remote Sensing of Environment*, **44**, pp. 144–163.

KRUSE, F.A., LEFKOFF, A.B. and DIETZ, J.B., 1993b, Expert system-based mineral mapping in northern death valley, California/Nevada using the airborne visible/infrared imaging spectrometer (AVIRIS). *Remote Sensing of Environment*, **44**, pp. 309–336.

KRUSE, F.A. and PERRY, S.L., 2009, Improving multispectral mapping by spectral modeling with hyperspectral signatures. *Journal of Applied Remote Sensing*, **3**, 22 p.

KRUSE, F.A., WEATHERBEE, O., PEPPIN, W., BIDELL, R., CALVIN, W. and TARANIK, J.V., 2010a, HSI mineral mapping from airborne, outcrop, and drill-core perspectives. In *Proceedings of the SPIE Symposium on Defense & Security*, 5–9 April 2010, Orlando, FL (Bellingham, WA: The International Society for Optical Engineering), Vol. 7687.

KRUSE, F.A., WEATHERBEE, O., PEPPIN, W., BIDELL, R., CALVIN, W. and TARANIK, J.V., 2010b, Use of an imaging spectrometer (hyperspectral system) to map alteration minerals at prospect, outcrop, and drill core scales. In *Proceedings of the Short Course in Remote Sensing and Spectral Geology, Geological Society of Nevada 2010 Symposium, Great Basin Evolution and Metallogeny, John Asuaga's Nugget Hotel*, 20–21 May 2010, Sparks, NV.

KURZ, T.H., BUCKLEY, S.J., HOWELL, J.A. and SCHNEIDER, D., 2008, Geological outcrop modelling and interpretation using ground based hyperspectral and laser scanning data fusion. *International Archives of the Photogrammetry, Remote Sensing and Spatial Information Sciences*, **37**, pp. 1229–1234.

KURZ, T.H., BUCKLEY, S.J., HOWELL, J.A. and SCHNEIDER, D., 2009, Close range hyperspectral and lidar data integration for geological outcrop analysis. In *Proceedings of the First Workshop on Hyperspectral Image and Signal Processing: Evolution in Remote Sensing (WHISPERS '09)*, 26–28 August 2009, Grenoble, France (New York: Institute of Electrical and Electronics Engineers), pp. 1–4.

MARTINEZ-ALONSO, S., RUSTAD, J.R. and GOETZ, A.F.H., 2002, Ab initio quantum mechanical modeling of infrared vibrational frequencies of the OH group in dioctahedral phyllosilicates. Part II: main physical factors governing the OH vibrations. *American Mineralogist*, **87**, pp. 1224–1234.

MATTHEW, M.W., ADLER-GOLDEN, S.M., BERK, A., FELDE, G., ANDERSON, G.P., GORODETZKY, D., PASWATERS, S. and SHIPPERT, M., 2003, Atmospheric correction of spectral imagery: evaluation of the FLAASH algorithm with AVIRIS data. In *SPIE Proceedings, Algorithms and Technologies for Multispectral, Hyperspectral, and Ultraspectral Imagery IX*, Orlando, FL (Bellingham, WA: The International Society for Optical Engineering), pp. 474–482.

MAUGER, A.J., 2007, *Mapping regional alteration patterns using hyperspectral drillcore scanner*, ASEG Extended Abstracts 2007 (Collingwood, VIC: CSIRO Publishing), pp. 1–3. Available online at: http://www.publish.csiro.au/?act=view_file&file_id=ASEG2007ab086.pdf (accessed 19 July 2011).

RICHTER, R. and SCHLÄPFER, D., 2002, Geo-atmospheric processing of airborne imaging spectrometry data. Part 2: atmospheric/topographic correction. *International Journal of Remote Sensing*, **23**, pp. 2631–2649.

SALISBURY, J.W., WALTER, L.S., VERGO, N. and D'ARIA, D.M., 1991, *Infrared (2.1–25 Micrometers) Spectra of Minerals*, 294 p. (Salisbury: Johns Hopkins University Press).

SWAYZE, G.A., CLARK, R.N., PEARSON, R.M. and LIVO, K.E., 1996, Mapping acid-generating minerals at the California Gulch Superfund site in Leadville, Colorado using imaging spectroscopy. In *Proceedings of the Seventh AVIRIS Airborne Geoscience Workshop*, 12–14 January 1998 (Pasadena, CA: Jet Propulsion Laboratory), pp. 231–234.

TARANIK, J.V. and ASLETT, Z.L., 2009, Development of hyperspectral imaging for mineral exploration. *Reviews in Economic Geology*, **16**, pp. 83–95.